

Article

Exploring the Iron Oxide Functionalized Biobased Carbon-silica-polyethyleneimine Composites for Hexavalent Chromium Removal from Dilute Aqueous Solutions

Mpho Cynthia Qhubu¹, Philiswa Nosizo Nomngongo²  and Vusumzi Emmanuel Pakade^{1,*} 

¹ Department of Chemistry, Faculty of Applied and Computer Sciences, Vaal University of Technology, Private Bag x 021, Vanderbijlpark 1900, South Africa; 213102382@edu.vut.ac.za

² Department of Science and Innovation (DSI)/National Research Foundation (NRF) South African Research Chair Initiative (SARChI), Nanotechnology for Water, University of Johannesburg, Johannesburg 2711, South Africa; pnnomngongo@uj.ac.za

* Correspondence: vusumzip@vut.ac.za; Tel.: +27-16-950-6629

Abstract: The contamination of water resources by toxic hexavalent chromium remains a challenge. In this study, amino-functionalized iron oxide biobased carbon-silica composites were prepared through co-precipitation of Fe(II) and Fe(III) over *Macadamia* activated carbon and explored as feasible adsorbents for the removal of Cr(VI) from dilute aqueous solutions. The energy dispersive spectroscopy (EDS) elemental analysis confirmed the existence of Fe, Si, O, and C atoms, which form the backbone of the composite. The FTIR also showed the presence of Fe-O and Si-O-Si and Si-OH spectral bands, affirming the backbone of the adsorbents. Cr(VI) adsorption efficiency (5.76 mg/g) was achieved at pH 1 when an initial concentration of 2.5 mg/L, contact time of 90 min, and dosage concentration of 1.7 g/L were used. The data were best described by the Langmuir adsorption model and pseudo-second-order rate model. ΔG° (−3 to −12 kJ/mol) and ΔH° (46, 12 and 5 kJ/mol) values affirmed that the adsorption of Cr(VI) was spontaneous and endothermic and dominated by chemical interactions.

Keywords: adsorption; activated carbon; co-precipitation; functionalization; iron oxide; chromium(VI)



Citation: Qhubu, M.C.; Nomngongo, P.N.; Pakade, V.E. Exploring the Iron Oxide Functionalized Biobased Carbon-silica-polyethyleneimine Composites for Hexavalent Chromium Removal from Dilute Aqueous Solutions. *Water* **2021**, *13*, 3081. <https://doi.org/10.3390/w13213081>

Academic Editor: Laura Bulgariu

Received: 26 August 2021

Accepted: 21 October 2021

Published: 2 November 2021

Publisher's Note: MDPI stays neutral with regard to jurisdictional claims in published maps and institutional affiliations.



Copyright: © 2021 by the authors. Licensee MDPI, Basel, Switzerland. This article is an open access article distributed under the terms and conditions of the Creative Commons Attribution (CC BY) license (<https://creativecommons.org/licenses/by/4.0/>).

1. Introduction

Chromium, similar to other heavy metals, is a menace to the environment as it persists and is non-biodegradable [1]. Chromium can be present in both anionic and cationic forms in aqueous media depending on the pH/Eh conditions. In cationic form, Cr(III) is the most stable oxidation state. At trace concentrations, Cr(III) is a micronutrient required by animals and humans [2]. The anionic chromium, Cr(VI), because of its carcinogenic and genotoxic properties, is classified as the 17th most toxic hazardous substance in the environment by the Agency for Toxic Substances and Disease Registry. The major sources of Cr(VI) in the environment are through anthropogenic activities because the kinetic reactions governing the conversion of natural Cr(III) to Cr(VI) are very slow [3,4]. In particular, Cr(VI) is a major element for the electroplating and stainless-steel production industries [5]. These industries use lots of water during their production, hence, the probability of Cr(VI) compounds leaching to the environment is too high [6]. Industrial wastewater containing chromium concentrations in the range of 0.5 to 270 mg/L have been reported [7]. The World Health Organization put stringent regulations to limit the amount of Cr(VI) in drinking water and surface water to 0.05 mg/L and 0.1 mg/L, respectively [6].

On one hand, current treatment techniques for the elimination of toxic Cr(VI) from water, which include ion exchange, membrane separation, and chemical precipitation, have limitations [8–10]. Membrane technology suffers from clogging and fouling [11], ion exchange is limited by high costs and fouling of resins [10], and chemical precipitation is

made difficult by the generation of toxic sludge which is costly to dispose of [12]. Adsorption on the other hand is highly favored due to simplicity in its design, ease of operation, low cost, low energy inputs, and use of cost-effective adsorbents [5,13]. However, its cost-effectiveness is dependent on the adsorbent being used, and its regeneration capabilities.

Biobased carbons, such as activated carbons (ACs), are widely used in the industry on a large scale as adsorbents for water purification, catalytic processes, and separation processes [14]. Activated carbons are applied in adsorption processes because of their large surface area, porous structure, and low cost of preparation [14–16]. Although efficient adsorption capacities have been reported for the removal of Cr(VI) using powdered ACs [17], challenges of separating the adsorbent from the solution have risen concerns of spent carbons being potential secondary pollutants.

The use of iron-based adsorbents in the removal of hexavalent chromium from aqueous solutions has attracted considerable research interest because of their power to transform Cr(VI) into Cr(III) during removal [18,19]. However, the iron-based materials have a shortfall of being applicable in a limited pH range due to precipitation of iron, and to address that, SiO₂ is often coated on the materials for applicability in a wider pH range [18]. Inorganic silica (SiO₂) is widely employed as a supporting material due to its favorable characteristics of being stable under acidic conditions, its inertness to redox reaction, and its high content of hydroxyl groups on its surface which allows further functionalization, ease of binding, and attachment of ligands [20].

Amino functionalized materials such as *m*-phenylenediamine, polyethyleneimine (PEI), polypyrrole (PPy), CM-dextran, and chitosan have also been explored as supporting materials for nanoparticles owing to their low cost of preparations and operations, porous structures, environmental stability, and regeneration properties [21]. The high content of deprotonated amine groups is critical for the adsorption of trace metal ions through electrostatic interactions and hydrogen bonding [22]. However, metal ions such as Cr(VI) undergo reductive transformation upon contact with electron donors to yield less toxic Cr(III) ions [23]. Immobilization of the formed-Cr(III) is also possible because the amino groups act as Lewis bases and form complexes with the Cr(III) [21]. The latter prepares the adsorbents via the functionalization of PEI to be of particular interest to researchers because both the adsorption and reduction mechanisms can be explored for the removal of Cr(VI). As such, adsorbents prepared by functionalization of PEI on a substrate have been widely used in the literature for the removal of Cr(VI) [24–29]. However, none of these were prepared from silica supported on biobased carbons originating from *Macadamia* nutshells. This study aimed to synthesize the iron oxide functionalized biobased carbon–silica–polyethyleneimine composites for the abatement of Cr(VI) in dilute aqueous solutions. The one-variable-at-a-time approach was used to study the effect of time, temperature, mass, concentration, and pH in batch mode.

2. Experimental Methods

2.1. Chemical Reagents

Potassium hydroxide (KOH), sodium hydroxide (NaOH), hydrochloric acid (32% HCl), sulfuric acid (98% H₂SO₄), iron (III) chloride (FeCl₃·6H₂O), iron (II) chloride (FeCl₂·4H₂O), potassium dichromate (K₂Cr₂O₇), 1,5'-diphenylcarbazine (DPC), ethanol, tetraethyl orthosilicate (TEOS), *N,N'*-dimethylformamide (DMF), acetic acid, 3-glycidyloxypropyltrimethoxysilane (GPS), and branched polyethyleneimine Mw = 2500 (PEI) were purchased from LabChem and Merck Chemical Co. (Johannesburg, South Africa) and were used without further purification. All chemicals were of reagent grade purity. Commercial *Macadamia* activated carbon was supplied by Innovation Carbon Pty LTD (Johannesburg, South Africa). The water used in this study for the preparation of stock, calibration standard, and working solutions was purified using Siemens LaboStar equipment (Warrendale, PA, USA). Duplicate batch adsorption experiments were conducted on a Scientech Ultrasonic Bath 703 supplied by Labotec (Johannesburg, South Africa). HI 2210 from Hanna Instruments (Johan-

nesburg, South Africa) was used to adjust the pH of solutions using diluted hydrochloric acid and sodium hydroxide solutions.

2.2. Preparation of Adsorbents

(i) Hydroxylation of AC

Macadamia activated carbon (AC) (150–300 μm) was firstly pre-treated in 5 mol/L KOH to achieve more porosity and possibly introduce OH^- groups on its surface for ease of binding and functionalization. The resultant product was then filtered and washed several times with ultrapure water. The product was further neutralized by washing with 1% acetic acid, then dried in an oven at 60 $^\circ\text{C}$ for 24 h and finally labeled AC-KOH.

(ii) Preparation of iron oxide modified AC (AC- Fe_3O_4)

Iron oxide was immobilized on the carbon surface through a co-precipitation method by dissolving a known amount of $\text{FeCl}_3 \cdot 6\text{H}_2\text{O}$ and $\text{FeCl}_2 \cdot 4\text{H}_2\text{O}$ salts in 300 mL ultrapure water and refluxed at 70 $^\circ\text{C}$ under a nitrogen flow for 2 h. About 5 g of AC-KOH was added to the $\text{Fe}^{2+}/\text{Fe}^{3+}$ solution to obtain a 1:1 ratio and stirred for half an hour while maintaining the pH between 10 and 11 using 5 mol/L NaOH solution. The solid material was separated by filtration, then washed several times with ultrapure water and ethanol and dried at 60 $^\circ\text{C}$ overnight.

(iii) Preparation of AC- Fe_3O_4 - SiO_2

The method reported by [30] was used to prepare the silica-coated biobased carbon. About 5 g of the recovered AC- Fe_3O_4 was refluxed in a 500 mL water and ethanol solution of 4:1 ratio at 60 $^\circ\text{C}$ under nitrogen flow. Tetraethyl orthosilicate (TEOS) was added dropwise to the solution to form AC- Fe_3O_4 - SiO_2 maintaining the pH in basic conditions (pH 9 to 11). The formed product AC- Fe_3O_4 - SiO_2 was separated by filtration, washed several times with ultrapure water and ethanol, and dried at 60 $^\circ\text{C}$ overnight.

(iv) Preparation of amino-modified adsorbent (AC- Fe_3O_4 - SiO_2 -PEI)

To bind the PEI ligand on AC- Fe_3O_4 - SiO_2 , the material was first hydroxylated using a method reported by [20] to increase the density of hydroxyl groups on the adsorbent surface. A 500 mL piranha solution (3:1 v/v H_2SO_4 : H_2O_2) was prepared and allowed to cool for 24 h. About 5 g of AC- Fe_3O_4 - SiO_2 was then added to the cooled piranha solution and sonicated for 10 min under nitrogen flow. The solid sample was then separated by centrifuge and washed several times with ultrapure water and ethanol followed by drying at 60 $^\circ\text{C}$ for 12 h. To the solid sample, 10 mL of 3-glycidyloxypropyltrimethoxysilane (GPS) and 20 mL toluene were added and stirred at 70 $^\circ\text{C}$ for 8 h under nitrogen flow. The adsorbent was separated from the solution by a centrifuge, washed several times with ultrapure water and ethanol, and dried at 60 $^\circ\text{C}$ overnight. About 5 g of GPS-treated AC- Fe_3O_4 - SiO_2 was refluxed in a 5% solution of branched polyethyleneimine (PEI) 100 mL at 70 $^\circ\text{C}$ for 12 h. The material was filtered and washed several times with ultrapure water and ethanol, then dried at 60 $^\circ\text{C}$ in an oven overnight. The resultant product was designated AC- Fe_3O_4 - SiO_2 -PEI.

2.3. Adsorption Experiments

Batch adsorption experiments were performed using AC- Fe_3O_4 , AC- Fe_3O_4 - SiO_2 , and AC- Fe_3O_4 - SiO_2 -PEI in duplicate for the adsorption of Cr(VI). Parameters such as solution pH (1–12), contact time (5–150 min), initial Cr(VI) concentration (1–12.5 mg/L), mass of adsorbent (0.05–3.0 g) and temperature (25, 35 and 45 $^\circ\text{C}$) were investigated by varying one parameter at a time while keeping others constant. Diluted solutions (0.1 mol/L) of HCl and NaOH were used to adjust the pH of the solution. An ultrasonicator (Scientech ultrasonic cleaner 703) set at low-frequency H1 was used for agitation and contact between the adsorbent and Cr(VI) solution. The total chromium and chromium (VI) remaining after adsorption were determined using a flame atomic absorption spectroscopy (AA-7000 Shimadzu, Kyoto, Japan), and UV-Vis spectrophotometer (Evolution 220, ThermoScientific,

Johannesburg, South Africa), respectively. The Cr(VI) complex was developed by reacting 0.1 mol/L of 1,5'-diphenylcarbazide solution in 10% sulfuric acid solution and the purplish solutions were analyzed with the UV-Vis at a wavelength of 540 nm. The adsorption capacity (q_e) and percent (%R) removal and were calculated using Equations (1) and (2), respectively.

$$q_e = \frac{V(C_o - C_e)}{W} \quad (1)$$

$$\% \text{ Removal} = \frac{(C_o - C_e)}{C_o} \cdot 100 \quad (2)$$

where C_o is the analyte initial concentration (mg/L), C_e is the final concentration (mg/L), M is the mass of the adsorbent (g) and V is the volume of the eluent (L).

2.4. Adsorption Isotherms

The Langmuir (Equation (3)), Freundlich (Equation (4)), and Dubinin-Radushkevich (Equation (5)) adsorption isotherms were used to deduce the removal mechanisms, the adsorption affinity and intensity of adsorption for Cr(VI) onto AC-Fe₃O₄, AC-Fe₃O₄-SiO₂, and AC-Fe₃O₄-SiO₂-PEI adsorbents. The equilibrium data were fitted into nonlinear models, as illustrated in Equations (3)–(5). The two well-known two-parameter models describe the adsorption of adsorbates onto adsorbents in two distinct phenomena. The Langmuir isotherm predicts the adsorption to proceed by a monolayer attachment of adsorbate on a single binding site that is on a homogeneous adsorbent surface. The Langmuir further assumes that no interactive bonding between adsorbates from adjacent sites occurs [31]. Conversely, the Freundlich isotherm allows for the interaction of adsorbates from adjacent active sites to take place, thus resulting in a heterogeneous surface with a multi-layered coverage. The Dubinin–Radushkevich isotherm can be used to confirm if the adsorption process is through physical or chemical interactions.

$$q_e = \frac{q_{mL}bC_e}{(1 + bC_e)} \quad (3)$$

$$q_e = K_F C_e^{1/n} \quad (4)$$

$$q_e = q_{mDR} \exp \left\{ -K_{DR} \left[RT \ln \left(1 + \frac{1}{C_e} \right) \right]^2 \right\} \quad (5)$$

where b is the Langmuir isotherm constant (L/mg), q_{mL} is the adsorption capacity at equilibrium (mg/g), K_F is Freundlich constant (mg/g)(mg/L)^{-1/n}, n is the Freundlich adsorption intensity exponent (dimensionless), q_{mDR} is the Dubinin–Radushkevich adsorption capacity (mg/g), K_{DR} is the Dubinin–Radushkevich isotherm constant (mol²/kJ²), R is the gas constant (8.314 J/(mol K)) and T is temperature (K).

3. Results and Discussion

3.1. Adsorbent Characterization

Figure 1 displays the FTIR spectra of AC-Fe₃O₄, AC-Fe₃O₄-SiO₂, and AC-Fe₃O₄-SiO₂-PEI. The vibration of Fe-O stretch in Fe₃O₄ was observed at 533.99 cm⁻¹ together with the sp² C=C bonds of the active carbon at 441 to 406 cm⁻¹. Compared to AC-Fe₃O₄, new bands appeared in AC-Fe₃O₄-SiO₂ at 1054.45 cm⁻¹ assigned to the stretching vibrations of Si-O-Fe [21] and/or C-O-C [28], while those at 948.73 and 791.46 cm⁻¹ were assigned to the asymmetric and symmetric stretches of Si-O-Si of the SiO₂. The AC-Fe₃O₄-SiO₂-PEI exhibited a peak at 3289 cm⁻¹ assigned to the -OH stretch which overlaps with the NH-stretch of the amine groups of PEI and the peaks at 2932.34 and 2816.03 cm⁻¹ were assigned to the asymmetric and symmetric -CH₂- stretching vibrations of the ethyl groups on PEI branches [32]. The new peaks at 1658, 1570, and 1454 cm⁻¹ in AC-Fe₃O₄-SiO₂-PEI were assigned to the vibration of C=O (-CONH amide band I), C-N (amide band II), and N-H (amide band III) C-N stretch of amide, suggesting a covalent bonding of PEI to the

epoxide ring [21,28,33]. The C-O-C peak of AC-Fe₃O₄-SiO₂ at 1054.45 cm⁻¹ was replaced by two peaks of the primary amine groups of the PEI at 1092–1030 cm⁻¹, representing the stretching N-H bends [28]. This suggested that the C-O-C functionality participated in the bonding of PEI to AC-Fe₃O₄-SiO₂ [28]. Moreover, these findings revealed that the PEI was bonded on the SiO₂ [32]. Although the peak of the SiO₂ was replaced by the amine groups, the symmetric shifted Si-O-Si peak at 759.24 cm⁻¹ was still visible together with the vibrating stretches of the Fe-O at 559.94 cm⁻¹ [21].

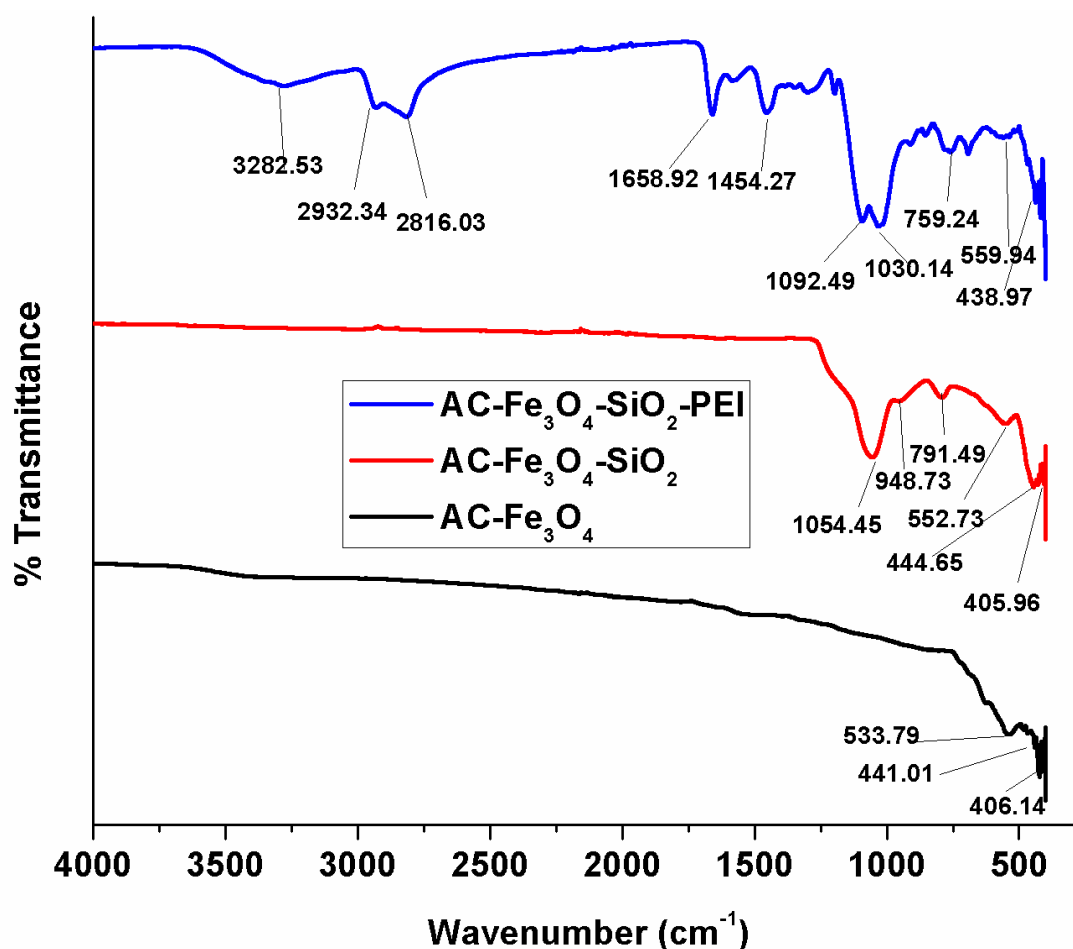


Figure 1. FTIR spectra of AC-Fe₃O₄, AC-Fe₃O₄-SiO₂, and AC-Fe₃O₄-SiO₂-PEI.

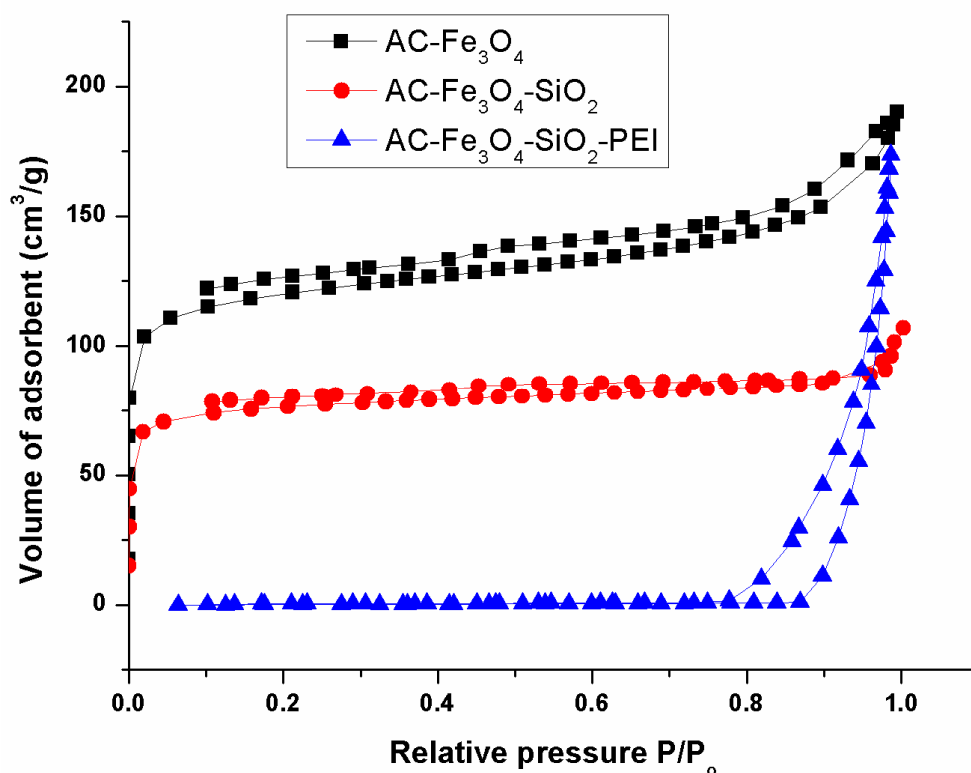
The elemental composition and specific surface area (S_{BET}) analyses of the prepared adsorbents together with that of AC reference material are shown in Table 1. The inclusion of Fe₃O₄ nanoparticles on AC lowered the %C from 83.27% to 44.03% and the S_{BET} surface area decreased from 546 to 386.89 m²/g. The decrease in %C was attributed to the presence of Fe, which is a much heavier atom than C, while the surface area reduction was probably due to the filling of AC pores by Fe₃O₄ nanoparticles or surface coverage through the formation of a semi-permeable layer of Fe₃O₄ on the AC surface. The atomic percent of C and H increased upon functionalization of AC-Fe₃O₄ by silica due to the attachment of CH₃CH₂- branches of the TEOS, but the surface area decreased to 234.51 m²/g. The %residual increased as functionalization occurred implying that other components except those of C, H, N, and S were present. The inclusion of an impervious layer of PEI on AC-Fe₃O₄-SiO₂ drastically decreased the BET value from 234.51 to 0.15 m²/g. Elsewhere, it was also observed that functionalization of AC with PEI led to a decrease in specific surface area from 942 to 32 m²/g due to surface passivation [34]. All the adsorbents had pore sizes ranging between 2 and 50 nm, signifying that the adsorbents had a mesoporous character as per the IUPAC categorization of pore sizes.

Table 1. Elemental analysis and surface characterization of adsorbents.

Adsorbents	Elemental Analysis					Surface Characterization		
	%C	%H	%N	%S	%R *	Surface Area (m ² /g)	Pore Volume (cm ³ /g)	Pore Size (nm)
AC	83.27	1.53	0.50	-	14.70	546.00	0.354	2.59
AC-Fe ₃ O ₄	44.03	1.41	0.25	<0.1	55.69	386.89	0.294	7.85
AC-Fe ₃ O ₄ -SiO ₂	68.30	1.79	0.44	<0.1	29.47	234.51	0.149	5.75
AC-Fe ₃ O ₄ -SiO ₂ -PEI	38.50	6.71	3.00	-	57.75	0.15	0.267	26.48

* R = residual (O, Fe, Si) calculated by difference.

The nitrogen adsorption-desorption plots are shown in Figure 2. These plots were used to determine the adsorption type and porosity structure of the adsorbent. AC-Fe₃O₄ and AC-Fe₃O₄-SiO₂ exhibited similar-shaped graphs. The graphs were of Type II adsorption isotherms hinting at a monolayer or multi-layered adsorption process. The graphs seemed to run parallel to P/P₀ at relative pressures below 0.9, in particular the AC-Fe₃O₄-SiO₂ and AC-Fe₃O₄-SiO₂-PEI, and then manifested a hysterical loop which suggested the formation of a microporous structure. AC-Fe₃O₄-SiO₂-PEI demonstrated a Type IV adsorption which is associated with capillary condensation of the mesoporous structure. A sharp hysterical loop at relatively low pressures represents adsorption-desorption hysteresis and is most common in oxide gels and mesoporous carbon materials [15].

**Figure 2.** N₂ adsorption/desorption isotherms of AC-Fe₃O₄, AC-Fe₃O₄-SiO₂, and AC-Fe₃O₄-SiO₂-PEI.

The X-ray-diffraction patterns for AC-Fe₃O₄, AC-Fe₃O₄-SiO₂, and AC-Fe₃O₄-SiO₂-PEI are presented in Figure 3. AC-Fe₃O₄ and AC-Fe₃O₄-SiO₂ exhibited six diffraction peaks at 2θ = 30°, 35°, 43°, 54°, 57°, and 63° which were related to 220, 311, 400, 511 and 440 crystal planes according to Bragg's reflection [16]. These diffraction peaks belong to the magnetite reference with a PDF card 19-0629 showing that Fe₃O₄ was successfully attached to the activated carbon [35]. The peak at 2θ of 35° in AC-Fe₃O₄-SiO₂-PEI was related to Bragg's reflection of 311 for the magnetite. This shows that even though the surface of the

AC was fully covered by the PEI, some Fe content was still present in the adsorbent. A large amorphous peak observed at $2\theta = 20^\circ$ in AC-Fe₃O₄-SiO₂-PEI was attributed to the amorphous structure of the PEI.

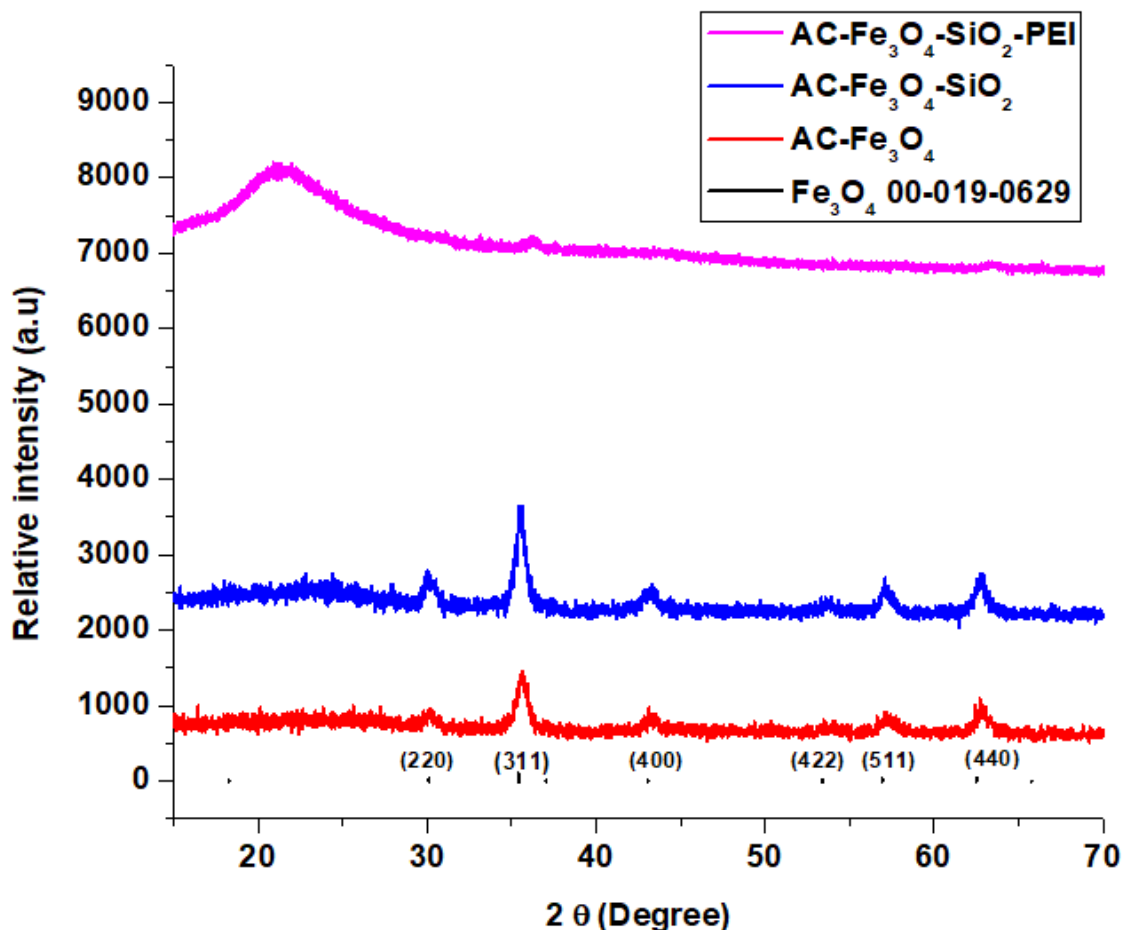


Figure 3. X-ray diffraction spectra of AC-Fe₃O₄, AC-Fe₃O₄-SiO₂, and AC-Fe₃O₄-SiO₂-PEI.

The SEM, TEM, and EDS graphs were used to study the morphology and elemental content of the prepared adsorbents (Figure 4). In the SEM image of AC-Fe₃O₄ shown in Figure 4a, small white precipitates of the Fe₃O₄ are observed as deposits in the large spherical pores of the AC. The EDS spectrum of AC-Fe₃O₄ in Figure 4b depicts the adsorbent to contain C, Fe, and O atoms in relative abundances of 62.2, 20.76, and 16.11 wt.%, respectively, among other things. The amorphousness observed in the SEM image of AC-Fe₃O₄-SiO₂ in Figure 4c was attributed to the deposition of silica to the AC-Fe₃O₄ surface, and this was confirmed by the elemental contents shown in the EDS spectrum (12.7 wt.% Si and 17.1 wt.% Fe) (Figure 4d). The increase in O atom abundance from 16.11 to 25.4 wt.% also corroborates the presence of SiO₂. Figure 4e,f depict the SEM and EDS spectral data of AC-Fe₃O₄-SiO₂-PEI. Irregular-shaped particles with smooth surfaces attributable to the gelatinous character of the PEI were observed. The EDS data (Figure 4f) confirmed the presence of C (51.0 wt.%), Fe (1.7 wt.%), and Si (12.1 wt.%) which formed the backbone of the adsorbent material. The C and O percent increased to 51.0 wt. % and 34.3 wt.%, respectively, signifying the presence of alkyl branched chains of PEI. The decrease in Fe content from 17.1 wt.% to 1.7 wt.% was attributed to leaching and oxidation of Fe₃O₄ as functionalization occurred. No N content was recorded on the EDS probably due to its lower atomic mass. The TEM images of AC-Fe₃O₄, AC-Fe₃O₄-SiO₂, and AC-Fe₃O₄-SiO₂-PEI are illustrated in Figure 5a–c. The darker shades in TEM were attributed to the presence of Fe₃O₄ while the lighter ones were due to AC backbone and silica.

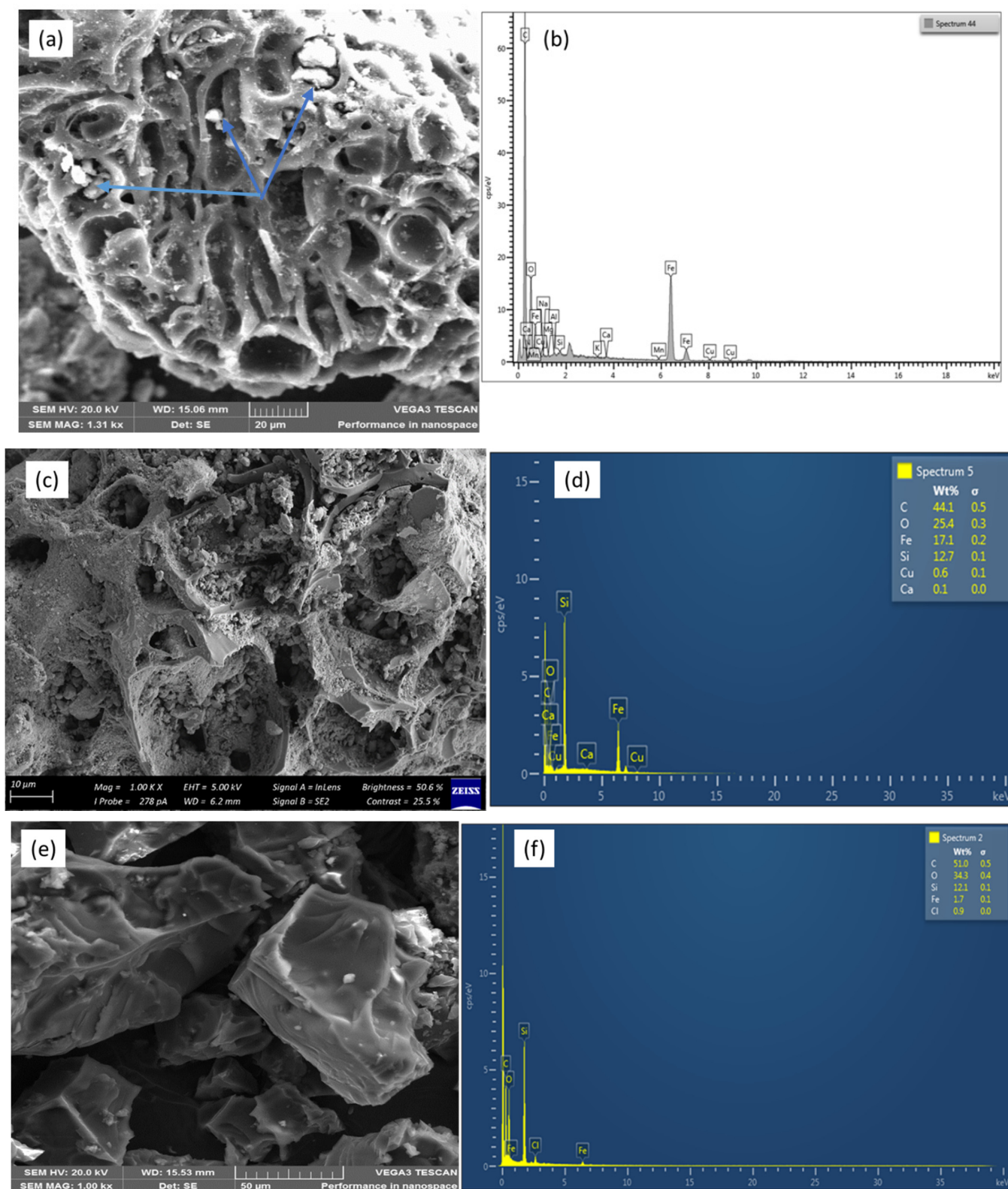


Figure 4. (a) SEM and (b) EDS of AC-Fe₃O₄, (c) SEM and (d) EDS of AC-Fe₃O₄-SiO₂; (e) SEM and (f) EDS of AC-Fe₃O₄-SiO₂-PEI.

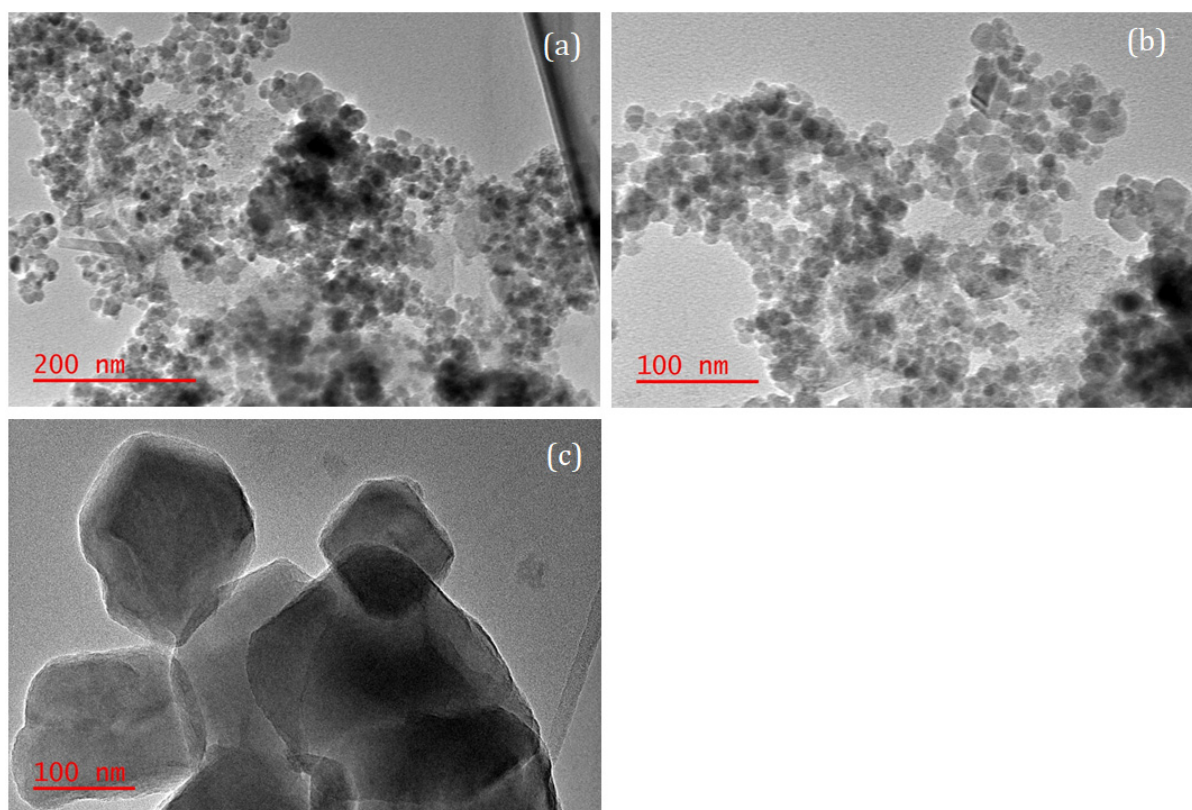


Figure 5. TEM images of AC-Fe₃O₄ (a), AC-Fe₃O₄-SiO₂ (b), and AC-Fe₃O₄-SiO₂-PEI (c).

Thermogravimetric analysis (TGA) and derivative thermogravimetric analysis (DTA) were used to study the thermal stability and decomposition stages of AC-Fe₃O₄, AC-Fe₃O₄-SiO₂, and AC-Fe₃O₄-SiO₂-PEI. The results are demonstrated in Figure 6. The decomposition curves exhibit different patterns as distinctly shown by the derivatives curves. However, some commonalities were observed, such as the decomposition stage taking place between 40 and 100 °C credited to moisture loss. This was quantified to 5, 5, and 10% weight loss for AC-Fe₃O₄, AC-Fe₃O₄-SiO₂, and AC-Fe₃O₄-SiO₂-PEI, respectively. The second weight loss was observed between 100 and 800 °C with 5% weight loss for AC-Fe₃O₄, between 100 and 300 °C for AC-Fe₃O₄-SiO₂ with 15% weight loss, and lastly between 300 and 600 °C for AC-Fe₃O₄-SiO₂-PEI with 40% weight loss. This stage was attributed to the loss of volatile compounds such as CO₂, CH₄, CO, and decomposition of adsorbents [36]. More of this weight loss was expressed with AC-Fe₃O₄-SiO₂ and AC-Fe₃O₄-SiO₂-PEI as compared to AC-Fe₃O₄. This was attributed to longer chains of CH₃CH₂- of the TEOS and those of the branched PEI. The last decomposition stage was attributed to the loss of lignin of the adsorbent which was more pronounced with AC-Fe₃O₄-SiO₂ and AC-Fe₃O₄-SiO₂-PEI than with AC-Fe₃O₄. Less weight loss observed by AC-Fe₃O₄ was attributed to the thermal stability of the Fe₃O₄ nanoparticles.

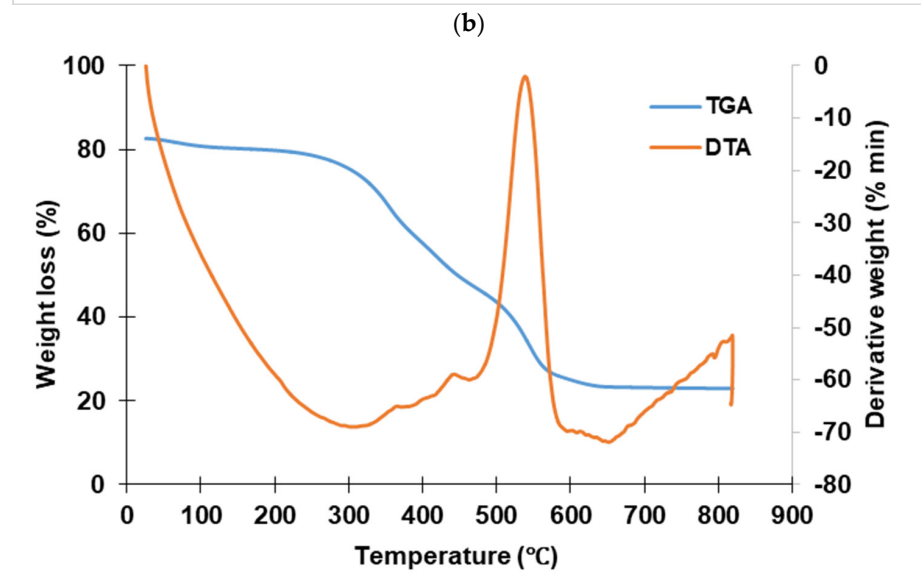
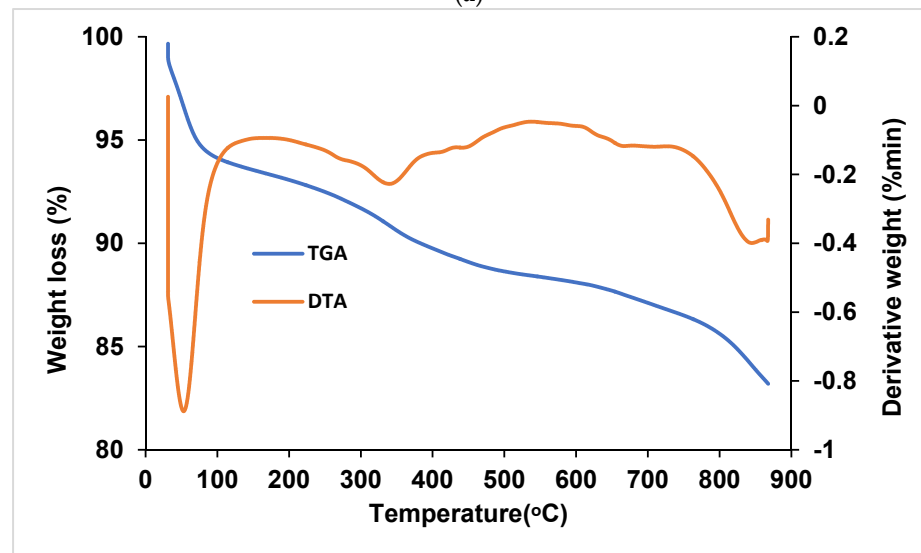
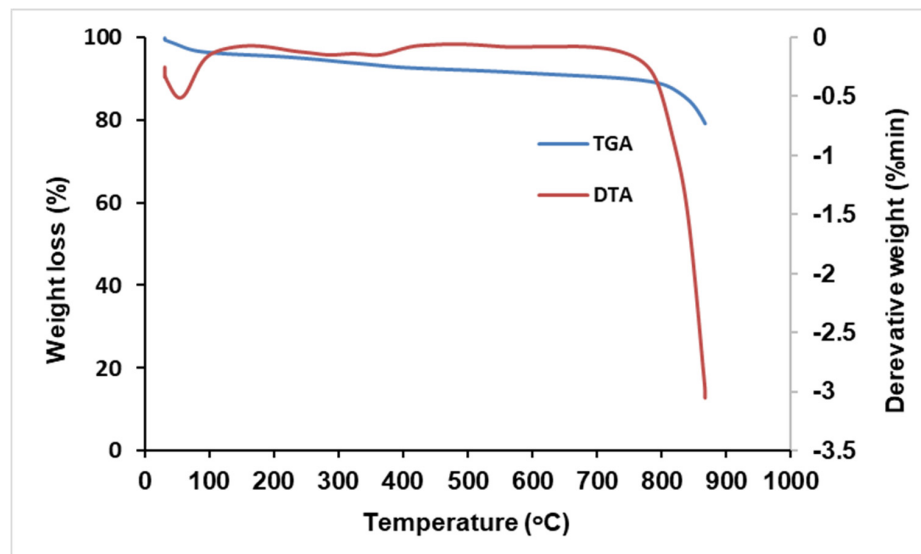


Figure 6. TGA and DTA of AC-Fe₃O₄ (a), AC-Fe₃O₄-SiO₂ (b), and AC-Fe₃O₄-SiO₂-PEI (c).

3.2. Influence of Solution pH on Adsorption of Cr(VI)

The zeta potential data of AC-Fe₃O₄, AC-Fe₃O₄-SiO₂, and AC-Fe₃O₄-SiO₂-PEI measured at different solution pH values are illustrated in Figure 7. The isoelectric point (IEP) can be determined from the graph as the pH point at which the surface charge of the adsorbent is zero or rather surface had electrical neutrality. It can be observed in Figure 7 that the zeta potential (mV) magnitude decreased with increasing solution pH for all adsorbents. At pH values below the IEP, the surface of the adsorbent is mostly positively charged and above IEP the surface is negatively charged [5,7,37]. The p*H*_{IEP} of AC-Fe₃O₄, AC-Fe₃O₄-SiO₂, and AC-Fe₃O₄-SiO₂-PEI was found to be 4.95, 3.53, and 11.69, respectively. The high IEP (pH 11.69) observed for AC-Fe₃O₄-SiO₂-PEI was attributed to the cationic characteristic of PEI [38,39].

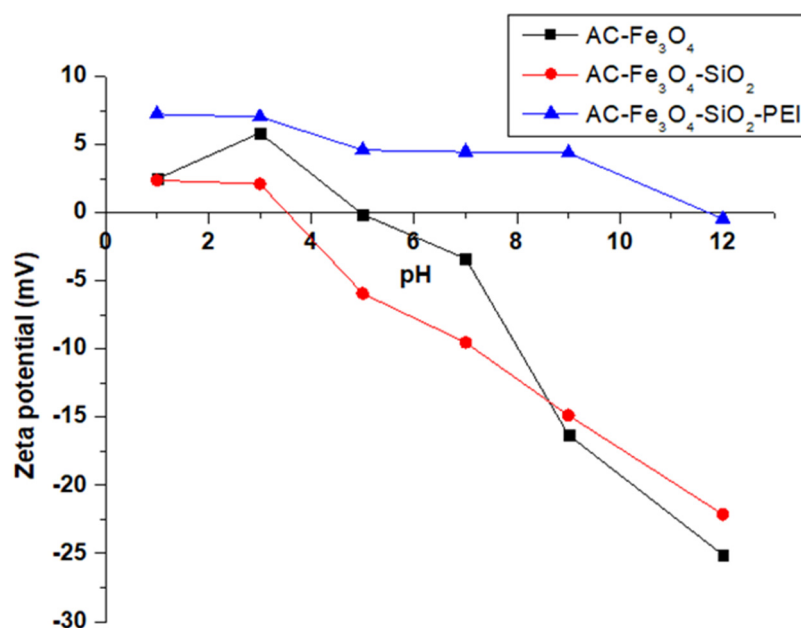


Figure 7. Zeta potential of AC-Fe₃O₄, AC-Fe₃O₄-SiO₂ and AC-Fe₃O₄-SiO₂-PEI.

The pH of a solution affects the surface chemistry of adsorbents, ionization, and bioavailability of adsorbates [25,40]. Hence, the investigation of its influence on adsorption is crucial. The influence of solution pH was investigated over the range of pH 1–12 and the result depicting the adsorption capacities against the pH is referred to in Figure 8a–c. All adsorbents exhibited a similar trend where the adsorption capacity of Cr(VI) decreased as the pH of the solution increased. The highest removal efficiencies were obtained between pH 1 and 3 for all three adsorbents. Explicitly, the optimum pH for AC-Fe₃O₄ (4.75 mg/g) was pH 3, and for both AC-Fe₃O₄-SiO₂ (4.47 mg/g) and AC-Fe₃O₄-SiO₂-PEI (3.63 mg/g), it was pH 1. The low removal efficiencies at high pH levels were attributed to forces of repulsion between negative sites on the adsorbent's surface and the anionic Cr(VI) ions in solutions. The negative sites on adsorbent surfaces are caused by the presence of a high concentration of OH[−] ions resulting from the NaOH solution used for the pH adjustments. In the case of AC-Fe₃O₄-SiO₂-PEI with high IEP at pH 11.69, the repulsion of Cr(VI) at high pHs could be due to the preferential binding of OH[−] groups to the cationic sites of adsorbents.

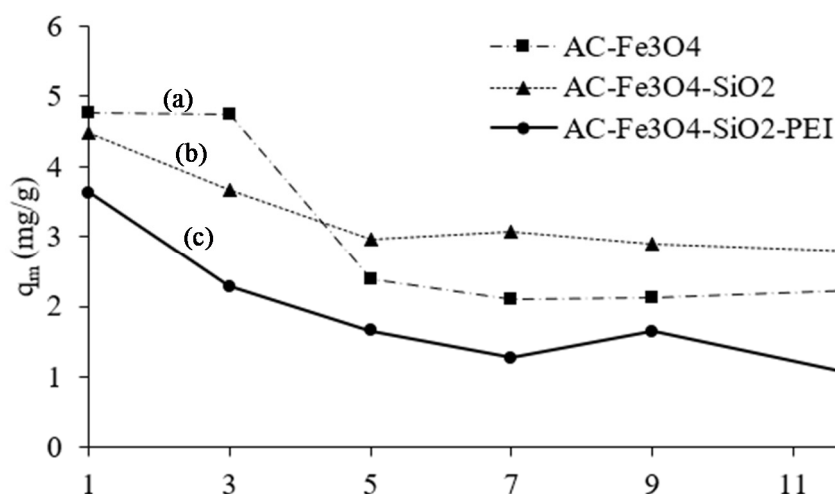


Figure 8. Effect of solution pH on the adsorption of Cr(VI) by AC-Fe₃O₄ (a), AC-Fe₃O₄-SiO₂ (b), and AC-Fe₃O₄-SiO₂-PEI (c). (conditions: 8 mg/L initial concentration 60 min contact time, 0.05 g adsorbent mass, 25 °C temperature and 30 mL solution volume).

The stability of the oxyanion character of Cr(VI) in solution is dependent on the solution pH, thus, the predominating species in acidic media (pH 1–5) is mostly HCrO₄[−], which is yielded by the hydrolysis of the dichromate ion (Cr₂O₇^{2−}) [25]. The oxyanions (HCrO₄[−], CrO₄^{2−} and Cr₂O₇^{2−}) at acidic conditions turn to become electrostatically attracted to the positively charged surface functional groups of the adsorbent [41]. The positive surface functional groups may be the results of protonation of NH₂, COOH, OH- functional groups on the surface of the adsorbents to form NH₃⁺, COOH²⁺, OH⁺ [36,42]. Because these functional groups are rich in electrons, it is possible that during Cr(VI) adsorption, some portion of the Cr(VI) is transformed to Cr(III) through receiving electrons from, for example, NH₂. In addition to the electrostatic attraction of Cr(VI) to the positively charged functional groups of the adsorbents at low acidic solutions, the reduction of Cr(VI) to Cr(III) due to the presence of electron-donating groups such as OH, NH₂, SH, COOH, and the oxidation of Fe²⁺ to Fe³⁺ are the other possible mechanisms for Cr(VI) removal by the prepared adsorbents [43]. The higher removal exhibited by AC-Fe₃O₄ compared to AC-Fe₃O₄-SiO₂ and AC-Fe₃O₄-SiO₂-PEI at acidic conditions could be attributed to the effects of adsorption and reduction of Cr(VI) to Cr(III) by Fe²⁺ ions on the surface of AC-Fe₃O₄ [37,44]. The same can be said of silica-containing adsorbent (AC-Fe₃O₄-SiO₂). The presence of PEI could enhance the repulsion of Cr(VI) due to hydrophobicity of PEI, hence low adsorption. At basic pH conditions, the amino groups of the PEI may attract the OH[−] through hydrogen bonding (R-NH₂—OH[−]), thus rendering the surface of adsorbent more electronegative, resulting in the repulsion of chromate ions and less adsorption effectiveness [42]. Moreover, the competition for adsorption sites between OH[−] and CrO₄^{2−} at higher pH (pH>6) has been reported by numerous researchers [7,40,45]. From pH 4 onwards, AC-Fe₃O₄ appears to have inferior performance compared to AC-Fe₃O₄-SiO₂, probably due to preferential binding of OH[−] by the exposed Fe²⁺/Fe³⁺ ions on AC-Fe₃O₄.

3.3. Adsorption Isotherms

The equilibrium sorption data of Cr(VI) on AC-Fe₃O₄ at 45 °C, AC-Fe₃O₄-SiO₂ at 45 °C, and AC-Fe₃O₄-SiO₂-PEI at 45 °C were fitted into Langmuir and Freundlich isotherm models to infer the type of interactions between the adsorbate and the adsorbents. The results are illustrated in Figure 9 and further summarized in Table 2. In Figure 9a the approximation line of Langmuir was closer to the experimental data points as compared to the Freundlich estimation. The coefficient of determination (R²), residual standard error (RSE), and the adsorption capacity (q_m) were used to infer which isotherm model best fitted the results. The R² value for AC-Fe₃O₄ was 0.828 in Langmuir and 0.737 in Freundlich.

Similarly, the RSE values were 0.172 and 0.263 in Langmuir and Freundlich models, respectively. In this regard, the higher R^2 value and lower RSE in Langmuir concurred with the visual observation that the data were best described by a monolayer, adsorption phenomenon of Langmuir. Additionally, AC-Fe₃O₄-SiO₂ data fitted to the Langmuir model better using the same reasoning applied above. In addition, the experimental (q_e) and estimated (q_m) adsorption capacity values for AC-Fe₃O₄-SiO₂ were closer to each other for each respective adsorbent. However, the data for AC-Fe₃O₄-SiO₂-PEI seemed to follow a different trend, as depicted by its better fitting to Freundlich ($R^2 = 0.957$; low RSE of 0.043), which suggests the complex adsorption of Cr(VI) through a multilayer process.

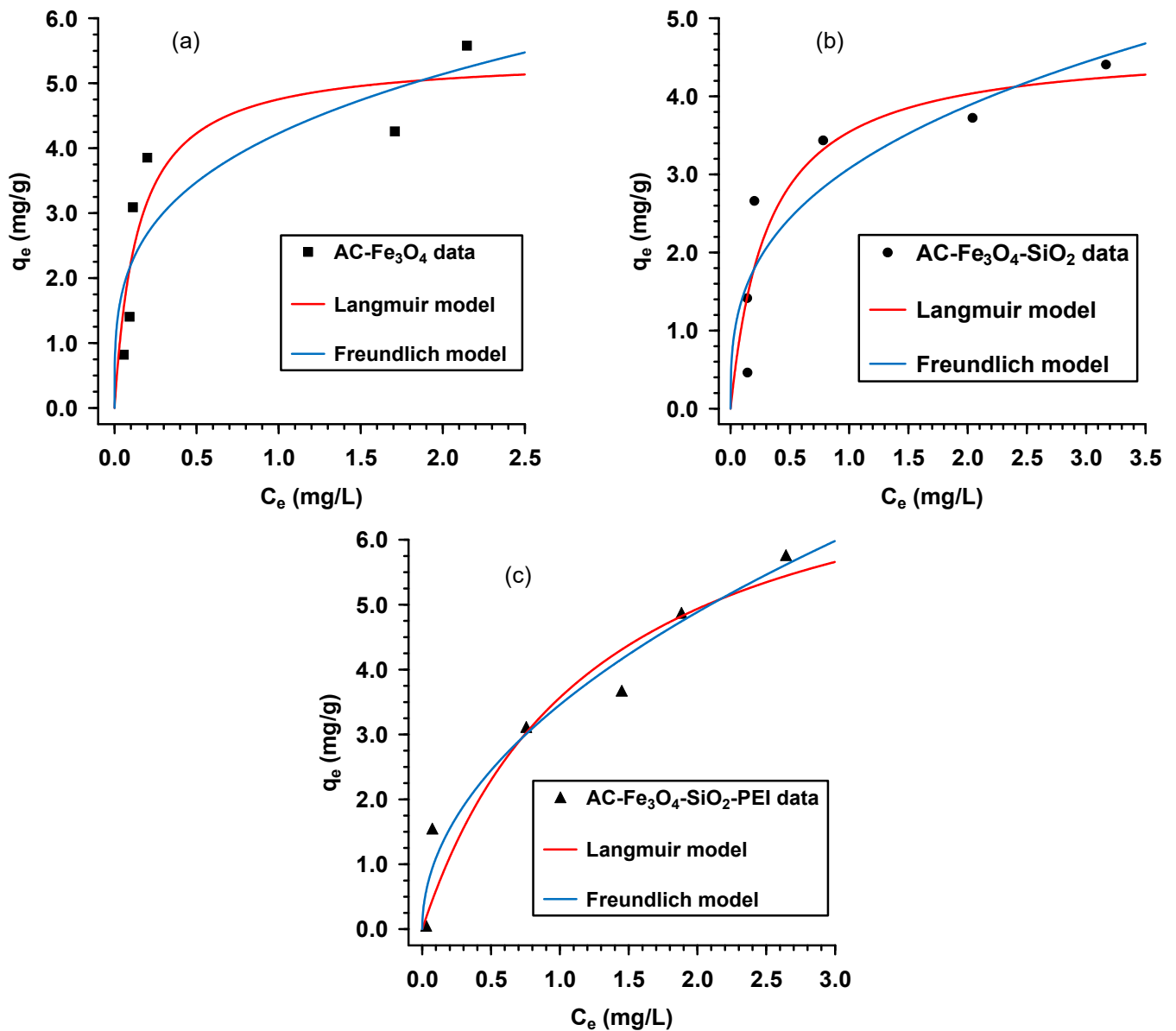


Figure 9. Isotherm modeling for the adsorption of Cr(VI) by AC-Fe₃O₄ (a), AC-Fe₃O₄-SiO₂ (b), and AC-Fe₃O₄-SiO₂-PEI (c) at 45 °C.

Table 2. The Freundlich and Langmuir adsorption isotherm parameters at 45 °C.

Isotherms	Parameters	AC-Fe ₃ O ₄	AC-Fe ₃ O ₄ -SiO ₂	AC-Fe ₃ O ₄ -SiO ₂ -PEI
Langmuir isotherm	q_{mL} (mg/g)	5.43	4.67	8.00
	b (L/mg)	7.07	3.16	0.80
	R ²	0.828	0.837	0.921
	RSE	0.172	0.163	0.079
Freundlich isotherm	n	3.55	2.99	2.00
	K_F (mg/g)(mg/L) ^{-1/n}	4.23	3.07	3.46
	R ²	0.737	0.778	0.957
	RSE	0.263	0.222	0.043
Dubinin-Radushkevich isotherm	q_{mDR} (mg/g)	5.23	4.22	4.72
	K_{DR} (mol ² /kJ ²)	0.02	0.04	0.03
	R ²	0.840	0.850	0.852
	RSE	0.160	0.150	0.148

3.4. Adsorption Kinetics

Pseudo-first-order (PFO) (Equation (6)) and pseudo-second-order (PSO) (Equation (7)) kinetic rate models were used to study the reaction kinetics for chromium (VI) adsorption by the three adsorbents (AC-Fe₃O₄, AC-Fe₃O₄-SiO₂, and AC-Fe₃O₄-SiO₂-PEI). The Elovich model was also fitted to the kinetic data to confirm the chemisorption nature of the adsorption process expressed using Equation (8).

$$q_t = q_e [1 - \exp(-k_1 t)] \quad (6)$$

$$q_t = \frac{tk_2 \cdot q_e^2}{(1 + k_2 t q_e)} \quad (7)$$

$$q_t = \frac{1}{\beta} \ln(1 + \alpha \beta t) \quad (8)$$

where q_t (mg/g) is the adsorption capacity of the adsorbent at time t , k_1 (1/min) and k_2 (g/mg/min) are the PFO and PSO rates constants, respectively. In Equation (8), β (mg/g) denotes the desorption rate, α (mg/g.min) is the initial adsorption rate and t is the time (min).

The data from fitting kinetics curves are referred to in Figure 10 and the numerical data is summarized in Table 3. The R² and RSE were used to decide on which model was best fitted to the experimental data. The high R² (0.949, 0.948, and 0.925) and low RSE (0.051, 0.052, and 0.075) values observed with the PSO model indicated its better fit compared to the PFO for AC-Fe₃O₄, AC-Fe₃O₄-SiO₂, and AC-Fe₃O₄-SiO₂-PEI, respectively. The Elovich error terms (R² and RSE) values were in agreement with the PSO data and suggested that chemisorption was the dominant mode of Cr(VI) removal. The high initial adsorption rates (α) show that the adsorption process was slow, probably due to the reaction being of chemical nature and poor porosity observed in Table 1.

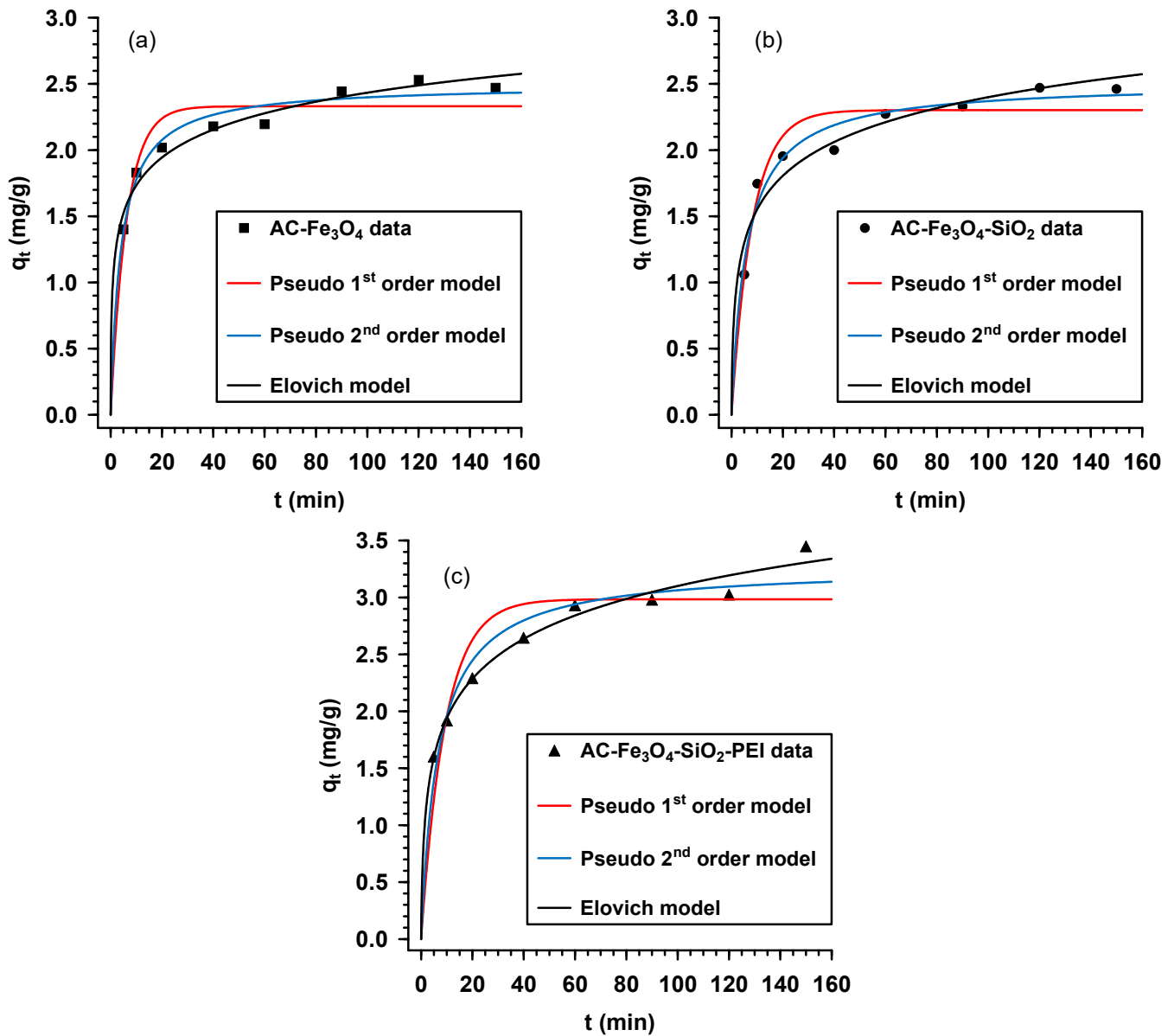


Figure 10. Kinetic modeling for the adsorption of Cr(VI) by AC-Fe₃O₄ (a), AC-Fe₃O₄-SiO₂ (b), and AC-Fe₃O₄-SiO₂-PEI (c).

Table 3. Kinetics isotherm parameters of AC-Fe₃O₄, AC-Fe₃O₄-SiO₂, and AC-Fe₃O₄-SiO₂-PEI.

Model	Parameters	AC-Fe ₃ O ₄	AC-Fe ₃ O ₄ -SiO ₂	AC-Fe ₃ O ₄ -SiO ₂ -PEI
Pseudo-first order	q_t (mg/g)	2.33	2.30	2.98
	k_1 (1/min)	0.16	0.12	0.11
	R^2	0.829	0.889	0.794
	RSE	0.171	0.111	0.206
Pseudo-second order	q_t (mg/g)	2.50	2.51	3.27
	k_2 ((g/(mg min)))	0.10	0.07	0.05
	R^2	0.949	0.948	0.925
	RSE	0.051	0.052	0.075
Elovich	α (mg/(g min))	8.98	2.41	2.25
	β (mg/g)	3.28	2.70	1.96
	R^2	0.953	0.914	0.978
	RSE	0.047	0.086	0.022

3.5. Performance Comparison

The Cr(VI) adsorption capacities of AC-Fe₃O₄, AC-Fe₃O₄-SiO₂, AC-Fe₃O₄-SiO₂-PEI were compared to similar materials found in the literature (Table 4). The adsorbents were compared based on initial solution pH, initial Cr(VI) concentration, and Langmuir adsorption capacity q_{mL} . Table 4 reveals that the adsorbents worked better at acidic conditions for the uptake of Cr(VI) from an aqueous solution. Numerous studies in the literature have reported the existence of electrostatic attraction forces between anionic Cr(VI) and positively charged adsorbent surface groups as the mode of the removal [33,46,47]. The initial concentration of Cr(VI), C_o , being studied varies as depicted in Table 3, depending on the type of water targeted for the clean-up. Those targeting wastewater normally use a high C_o concentration of Cr(VI), while those aiming for analysis of drinking water use low concentration. The selected iron oxide functionalized materials presented in Table 4 also reveal that producing these types of materials that possess high adsorption capacity values presents a challenge [48]. Based on this observation, it can be concluded that the materials produced in this study performed fairly well in comparison to the literature. Hence, the current material extends the research on the type of adsorbents that can be evaluated for Cr(VI) adsorption. It has been reported that despite the high content of amino groups on PEI, high loading of PEI may lead to reduced surface areas, which may lead to lower adsorption capacities [28]. Lower adsorption capacities were observed with PEI-loaded adsorbents as compared to magnetite-loaded AC due to reduced surface areas.

Table 4. Comparison of adsorption capacities of Cr(VI) by different adsorbents as to AC-Fe₃O₄, AC-Fe₃O₄SiO₂ and AC-Fe₃O₄-SiO₂-PEI.

Adsorbent	pH	C_o (mg/L)	q_{mL} (mg/g)	Reference
Magnetic biochar	3	100	8.35	[35]
MBC/PPy	3	10	19.23	[49]
Magnetic biochar (MMABC)	3	10	25.27	[50]
Fe ₃ O ₄ -PEI800-MNT	1–9	10–25	8.77	[51]
Fe ₃ O ₄ -PEI25000-MNT	1–9	10–25	7.69	[51]
AC-Fe ₃ O ₄	3	5	5.43	This study
AC-Fe ₃ O ₄ -SiO ₂	1	5	4.67	This study
AC-Fe ₃ O ₄ -SiO ₂ -PEI	1	5	8.00	This study

3.6. Thermodynamic Studies

The thermodynamic studies for the adsorption of Cr(VI) by AC-Fe₃O₄, AC-Fe₃O₄-SiO₂, and AC-Fe₃O₄-SiO₂-PEI adsorbents were evaluated at different temperatures (25, 35, and 45 °C) to predict the adsorption nature and spontaneity of the process. Parameters such as the entropy change (ΔS° , J/(mol K)), enthalpy change (ΔH° , J/mol), and Gibb's free energy (ΔG° , J/mol) were calculated by relating Gibb's free energy to the equilibrium constant K_c using Equations (9)–(12).

$$\Delta G^\circ = \Delta H^\circ - T\Delta S^\circ \quad (9)$$

$$\Delta G^\circ = -RT \ln K_c^\circ \quad (10)$$

$$K_c^\circ = \frac{Mw_{(HCrO_4^-)} \cdot 1000 \cdot b \cdot [HCrO_4^-]^\circ}{\gamma} \quad (11)$$

$$\ln \left(\frac{Mw_{(HCrO_4^-)} \cdot 1000 \cdot b \cdot [HCrO_4^-]^\circ}{\gamma} \right) = \frac{\Delta S^\circ}{R} - \frac{\Delta H^\circ}{RT} \quad (12)$$

where ΔG° is Gibb's free energy (J/mol), R is the universal gas constant (8.3144 J/mol K), K_c° is the dimensionless equilibrium constant, $Mw_{(HCrO_4^-)}$ is the molecular weight of model pollutant $HCrO_4^-$, γ is the coefficient of activity (dimensionless) [52], b is the Langmuir

isotherm constant (L/mg), $[HCrO_4^-]^0$ is the standard concentration of the adsorbate (1 mol/L) and T is the temperature (K).

The ΔG^0 , ΔH^0 and ΔS^0 results are stipulated in Table 5. The ΔG^0 values were found to be negative for AC-Fe₃O₄, AC-Fe₃O₄-SiO₂ and AC-Fe₃O₄-SiO₂-PEI at all temperatures investigated (298, 308, and 318 K). The values of ΔG^0 ranged between -17 and -36 kJ/mol, indicating a spontaneous adsorption process. The positive ΔH^0 values (871.45 kJ/mol for AC-Fe₃O₄-SiO₂-PEI) indicated that the Cr(VI) adsorption process was endothermic and fell outside the 2–30 kJ/mol range which is characteristic of chemisorption [49]. In addition, the positive ΔH^0 values are associated with the proven endothermic reaction of Cr(VI) to Cr(III) reduction [33,53]. The adsorption of Cr(VI) by AC-Fe₃O₄-SiO₂ and AC-Fe₃O₄-SiO₂-PEI was regarded as highly randomized, as the ΔS^0 values were above zero [54]. The adsorption of Cr(VI) using AC-Fe₃O₄-SiO₂ and AC-Fe₃O₄-SiO₂-PEI adsorbents was dominated by entropy change as opposed to enthalpy change due to $|T\Delta S^0| > |\Delta H^0|$ [55].

Table 5. Thermodynamics parameters of AC-Fe₃O₄, AC-Fe₃O₄-SiO₂, and AC-Fe₃O₄-SiO₂-PEI at different temperatures.

Adsorbent	T (K)	b (L/mg)	ln (K ⁰)	ΔG^0 (kJ/mol)	$ T\Delta S^0 $ (kJ/mol)	ΔH^0 (kJ/mol)	ΔS^0 (J/(mol K))
AC-Fe ₃ O ₄	298	20.85	14.71	-25.43	160.03	133.45	537.00
	308	5.51	13.38	-34.25	165.40		
	318	7.07	13.68	-36.17	170.77		
AC-Fe ₃ O ₄ -SiO ₂	298	5.44	13.36	-23.11	160.62	136.09	539.00
	308	3.10	12.80	-32.78	166.01		
	318	3.16	12.82	-33.89	171.40		
AC-Fe ₃ O ₄ -SiO ₂ -PEI	298	0.15	9.77	-16.90	881.63	871.45	2958.50
	308	0.25	10.28	-26.33	911.22		
	318	0.80	28.77	-76.07	940.80		

4. Conclusions

Amino functionalized activated carbon silica composites were prepared and explored as adsorbents for the removal of Cr(VI) from aqueous solutions. The FTIR analysis showed the presence of asymmetric and symmetric peaks of Fe-O, Si-O-Si, and Si-OH bonds at 533, 791, and 1054 cm⁻¹ alluding to the successful incorporation of Fe₃O₄ and SiO₂ on the surface of the AC. The EDS data further confirmed the presence of Fe, Si, O, and C atoms in proportional amounts on the adsorbents. Small deposits representing Fe₃O₄ precipitates were observed in the large pores of AC-Fe₃O₄ SEM images. The BET surface area of AC-Fe₃O₄ decreased from 387 to 0.15 m²/g following the attachment of SiO₂ and PEI to the biobased carbon. Attachment of SiO₂ on AC-Fe₃O₄ resulted in increased %C and %H correlating to the inclusion of CH₃-CH₂ chains of TEOS. The isoelectric points of AC-Fe₃O₄, AC-Fe₃O₄-SiO₂, and AC-Fe₃O₄-SiO₂-PEI were at pH 4.95, 3.53, and 11.69, respectively. The high positivity in isoelectric charge predicts increased electrostatic interaction between the positively charged adsorbent and negatively charged Cr(VI) ions. The batch adsorption experiments displayed optimum conditions of pH 3 and 1, initial concentration 5 mg/L, 0.15 g adsorbent mass, 120 min contact time, and 45 °C temperature. The experimental data were best fitted to Langmuir adsorption isotherm for all three prepared adsorbents, predicting that the adsorption process occurred over a homogenous, mono-layered coverage. The kinetics data were best fitted to the pseudo-second-order rate model. According to the thermodynamics parameters, the adsorption of Cr(VI) by the composites was spontaneous and endothermic. The high enthalpy change energy suggested chemical transformation of adsorbed Cr(VI) into Cr(III), thus overruling the physisorption as the dominant mechanism but chemisorption. Additionally, the poor porosity of the main sorbent favored the chemisorption uptake of Cr(VI). In comparison to similar adsorbents, the AC-Fe₃O₄, AC-Fe₃O₄-SiO₂, and AC-Fe₃O₄-SiO₂-PEI showed promising adsorption capacities and can be used as adsorbents for the removal of Cr(VI) from dilute aqueous solutions but adsorbents need improvement or testing using other pollutants like organic dyes.

Author Contributions: M.C.Q.: Investigation, Methodology, Data curation, Writing—Original draft preparation. P.N.N.: Supervision, Conceptualization, Methodology, Resources, Reviewing and Editing. V.E.P.: Conceptualization, Methodology, Software, Supervision, Funding acquisition, Reviewing and Editing. All authors have read and agreed to the published version of the manuscript.

Funding: The authors thank the financial support from the South African National Research Foundation (Grant numbers: TTK13061018779 and TTK16051164648).

Institutional Review Board Statement: Not applicable.

Informed Consent Statement: Not applicable.

Data Availability Statement: The data presented in this study are available on request from the corresponding author.

Acknowledgments: We thank Malvin Moyo for the technical support.

Conflicts of Interest: The authors declare no conflict of interest.

References

1. Heiderscheidt, E.; Postila, H.; Leiviskä, T. Removal of metals from wastewaters by mineral and biomass-based sorbents applied in continuous-flow continuous stirred tank reactors followed by sedimentation. *Sci. Total Environ.* **2020**, *700*, 135079. [[CrossRef](#)]
2. White, P.J.; Brown, P.H. Plant nutrition for sustainable development and global health. *Ann. Bot.* **2010**, *105*, 1073–1080. [[CrossRef](#)] [[PubMed](#)]
3. Bartlett, R.J. Chromium cycling in soils and water: Links, gaps, and methods. *Environ. Health Perspect.* **1991**, *92*, 17–24. [[CrossRef](#)] [[PubMed](#)]
4. Kumar, A.; Joseph, S.; Tsechansky, L.; Schreiter, I.J.; Schüth, C.; Taherysoosavi, S.; Mitchell, D.R.G.; Graber, E.R. Mechanistic evaluation of biochar potential for plant growth promotion and alleviation of chromium-induced phytotoxicity in *Ficus elastica*. *Chemosphere* **2020**, *243*, 125332. [[CrossRef](#)] [[PubMed](#)]
5. Pap, S.; Bezanovic, V.; Radonic, J.; Babic, A.; Saric, S.; Adamovic, D.; Turk Sekulic, M. Synthesis of highly-efficient functionalized biochars from fruit industry waste biomass for the removal of chromium and lead. *J. Mol. Liq.* **2018**, *268*, 315–325. [[CrossRef](#)]
6. Qiu, B.; Wang, Y.; Sun, D.; Wang, Q.; Zhang, X.; Weeks, B.L.; O'Connor, R.; Huang, X.; Wei, S.; Guo, Z. Cr(vi) removal by magnetic carbon nanocomposites derived from cellulose at different carbonization temperatures. *J. Mater. Chem. A* **2015**, *3*, 9817–9825. [[CrossRef](#)]
7. Rai, M.K.; Shahi, G.; Meena, V.; Meena, R.; Chakraborty, S.; Singh, R.S.; Rai, B.N. Removal of hexavalent chromium Cr (VI) using activated carbon prepared from mango kernel activated with H₃PO₄. *Resour. Technol.* **2016**, *2*, S63–S70. [[CrossRef](#)]
8. Corazza, M.Z.; Somera, B.F.; Segatelli, M.G.; Tarley, C.R.T. Grafting 3-mercaptopropyl trimethoxysilane on multi-walled carbon nanotubes surface for improving on-line cadmium(II) preconcentration from water samples. *J. Hazard. Mater.* **2012**, *243*, 326–333. [[CrossRef](#)]
9. Kononova, O.N.; Bryuzgina, G.L.; Apchitaeva, O.V.; Kononov, Y.S. Ion exchange recovery of chromium (VI) and manganese (II) from aqueous solutions. *Arab. J. Chem.* **2019**, *12*, 2713–2720. [[CrossRef](#)]
10. Mnif, A.; Bejaoui, I.; Mouelhi, M.; Hamrouni, B. Hexavalent Chromium Removal from Model Water and Car Shock Absorber Factory Effluent by Nanofiltration and Reverse Osmosis Membrane. *Int. J. Anal. Chem.* **2017**, *2017*, 7415708. [[CrossRef](#)]
11. Rol, F.; Belgacem, M.N.; Gandini, A.; Bras, J. Recent advances in surface-modified cellulose nanofibrils. *Prog. Polym. Sci.* **2019**, *88*, 241–264. [[CrossRef](#)]
12. Stylianou, S.; Simeonidis, K.; Mitrakas, M.; Zouboulis, A.; Ernst, M.; Katsoyiannis, I.A. Reductive precipitation and removal of Cr(VI) from groundwaters by pipe flocculation-microfiltration. *Environ. Sci. Pollut. Res.* **2018**, *25*, 12256–12262. [[CrossRef](#)] [[PubMed](#)]
13. He, R.; Yuan, X.; Huang, Z.; Wang, H.; Jiang, L.; Huang, J.; Tan, M.; Li, H. Activated biochar with iron-loading and its application in removing Cr (VI) from aqueous solution. *Colloids Surfaces A Physicochem. Eng. Asp.* **2019**, *579*, 123642. [[CrossRef](#)]
14. Miao, M.S.; Wang, Y.N.; Kong, Q.; Shu, L. Adsorption kinetics and optimum conditions for Cr(VI) removal by activated carbon prepared from luffa sponge. *Desalin. Water Treat.* **2016**, *57*, 7763–7772. [[CrossRef](#)]
15. Gottipati, R.; Mishra, S. Preparation of microporous activated carbon from Aegle Marmelos fruit shell and its application in removal of chromium(VI) from aqueous phase. *J. Ind. Eng. Chem.* **2016**, *36*, 355–363. [[CrossRef](#)]
16. Cai, W.; Li, Z.; Wei, J.; Liu, Y. Synthesis of peanut shell based magnetic activated carbon with excellent adsorption performance towards electroplating wastewater. *Chem. Eng. Res. Des.* **2018**, *140*, 23–32. [[CrossRef](#)]
17. Hlungwane, L.; Viljoen, E.L.; Pakade, V.E. Macadamia nutshells-derived activated carbon and attapulgite clay combination for synergistic removal of Cr(VI) and Cr(III). *Adsorpt. Sci. Technol.* **2018**, *36*, 713–731. [[CrossRef](#)]
18. Zeng, Q.; Huang, Y.; Huang, L.; Hu, L.; Xiong, D.; Zhong, H. Efficient removal of hexavalent chromium in a wide pH range by composite of SiO₂ supported nano ferrous oxalate. *Chem. Eng. J.* **2020**, *383*, 123209. [[CrossRef](#)]

19. Zeng, Q.; Huang, Y.; Wang, H.; Huang, L.; Hu, L.; Zhong, H. A novel composite of almandine supported humboldtine nanospheres, in situ synthesized from natural almandine, possesses high removal efficiency of Cr (VI) over a wide pH range. *J. Hazard. Mater.* **2020**, *383*, 121199. [[CrossRef](#)]
20. Ta, T.K.H.; Trinh, M.T.; Long, N.V.; Nguyen, T.T.M.; Nguyen, T.L.T.; Thuoc, T.L.; Phan, B.T.; Mott, D.; Maenosono, S.; Tran-Van, H.; et al. Synthesis and surface functionalization of Fe₃O₄-SiO₂ core-shell nanoparticles with 3-glycidoxypropyltrimethoxysilane and 1,1'-carbonyldiimidazole for bio-applications. *Colloids Surfaces A Physicochem. Eng. Asp.* **2016**, *504*, 376–383. [[CrossRef](#)]
21. Shi, S.; Yang, J.; Liang, S.; Li, M.; Gan, Q.; Xiao, K.; Hu, J. Enhanced Cr(VI) removal from acidic solutions using biochar modified by Fe₃O₄@SiO₂-NH₂ particles. *Sci. Total Environ.* **2018**, *628–629*, 499–508. [[CrossRef](#)]
22. Jiang, Y.; Liu, Z.; Zeng, G.; Liu, Y.; Shao, B.; Li, Z.; Liu, Y.; Zhang, W.; He, Q. Polyaniline-based adsorbents for removal of hexavalent chromium from aqueous solution: A mini review. *Environ. Sci. Pollut. Res.* **2018**, *25*, 6158–6174. [[CrossRef](#)]
23. Zeng, Q.; Hu, Y.; Yang, Y.; Hu, L.; Zhong, H.; He, Z. Cell envelop is the key site for Cr (VI) reduction by *Oceanobacillus oncorhynchii* W4, a newly isolated Cr (VI) reducing bacterium. *J. Hazard. Mater.* **2019**, *368*, 149–155. [[CrossRef](#)] [[PubMed](#)]
24. Mo, Y.; Wang, S.; Vincent, T.; Desbrieres, J.; Faur, C.; Guibal, E. New highly-percolating alginate-PEI membranes for efficient recovery of chromium from aqueous solutions. *Carbohydr. Polym.* **2019**, *225*, 115177. [[CrossRef](#)]
25. Zhang, S.; Wang, Z.; Chen, H.; Kai, C.; Jiang, M.; Wang, Q.; Zhou, Z. Polyethylenimine functionalized Fe₃O₄/steam-exploded rice straw composite as an efficient adsorbent for Cr(VI) removal. *Appl. Surf. Sci.* **2018**, *440*, 1277–1285. [[CrossRef](#)]
26. Moyo, M.; Modise, S.J.; Pakade, V.E. Palladium nanoparticles dispersed on functionalized macadamia nutshell biomass for formic acid-mediated removal of chromium(VI) from aqueous solution. *Sci. Total Environ.* **2020**, *743*, 140614. [[CrossRef](#)]
27. Tangtubtim, S.; Saikrasun, S. Adsorption behavior of polyethyleneimine-carbamate linked pineapple leaf fiber for Cr(VI) removal. *Appl. Surf. Sci.* **2019**, *467–468*, 596–607. [[CrossRef](#)]
28. Geng, J.; Yin, Y.; Liang, Q.; Zhu, Z.; Luo, H. Polyethyleneimine cross-linked graphene oxide for removing hazardous hexavalent chromium: Adsorption performance and mechanism. *Chem. Eng. J.* **2019**, *361*, 1497–1510. [[CrossRef](#)]
29. Liu, Y.; Hu, J.; Li, Y.; Wei, H.P.; Li, X.S.; Zhang, X.H.; Chen, S.M.; Chen, X.Q. Synthesis of polyethyleneimine capped carbon dots for preconcentration and slurry sampling analysis of trace chromium in environmental water samples. *Talanta* **2015**, *134*, 16–23. [[CrossRef](#)] [[PubMed](#)]
30. Fatehi, M.H.; Shayegan, J.; Zabihi, M.; Goodarznia, I. Functionalized magnetic nanoparticles supported on activated carbon for adsorption of Pb(II) and Cr(VI) ions from saline solutions. *J. Environ. Chem. Eng.* **2017**, *5*, 1754–1762. [[CrossRef](#)]
31. Al-Ghouti, M.A.; Da'ana, D.A. Guidelines for the use and interpretation of adsorption isotherm models: A review. *J. Hazard. Mater.* **2020**, *393*, 122383. [[CrossRef](#)] [[PubMed](#)]
32. Lee, M.Y.; Lee, J.H.; Chung, J.W.; Kwak, S.Y. Hydrophilic and positively charged polyethyleneimine-functionalized mesoporous magnetic clusters for highly efficient removal of Pb(II) and Cr(VI) from wastewater. *J. Environ. Manag.* **2018**, *206*, 740–748. [[CrossRef](#)]
33. Liang, X.; Fan, X.; Li, R.; Li, S.; Shen, S.; Hu, D. Efficient removal of Cr(VI) from water by quaternized chitin/branched polyethyleneimine biosorbent with hierarchical pore structure. *Bioresour. Technol.* **2018**, *250*, 178–184. [[CrossRef](#)]
34. Yin, C.Y.; Aroua, M.K.; Daud, W.M.A.W. Impregnation of palm shell activated carbon with polyethyleneimine and its effects on Cd²⁺ adsorption. *Colloids Surfaces A Physicochem. Eng. Asp.* **2007**, *307*, 128–136. [[CrossRef](#)]
35. Zhong, D.; Zhang, Y.; Wang, L.; Chen, J.; Jiang, Y.; Tsang, D.C.W.; Zhao, Z.; Ren, S.; Liu, Z.; Crittenden, J.C. Mechanistic insights into adsorption and reduction of hexavalent chromium from water using magnetic biochar composite: Key roles of Fe₃O₄ and persistent free radicals. *Environ. Pollut.* **2018**, *243*, 1302–1309. [[CrossRef](#)]
36. Lesaoana, M.; Mlaba, R.P.V.; Mtunzi, F.M.; Klink, M.J.; Edijike, P.; Pakade, V.E. Influence of inorganic acid modification on Cr(VI) adsorption performance and the physicochemical properties of activated carbon. *S. Afr. J. Chem. Eng.* **2019**, *28*. [[CrossRef](#)]
37. Li, B.; Zhang, L.; Yin, W.; Lv, S.; Li, P.; Zheng, X.; Wu, J. Effective immobilization of hexavalent chromium from drinking water by nano-FeOOH coating activated carbon: Adsorption and reduction. *J. Environ. Manag.* **2021**, *277*, 111386. [[CrossRef](#)]
38. Zhang, T.; Yue, X.; Zhang, K.; Li, J.; Zhu, C.; Zhang, L.; Chen, W. Selective adsorption of CuSO₄ from mixed sulfate solutions by Cu(II) ion-imprinted polymers containing salicylaldoximes, ammonium cations, and tertiary amino groups. *Mater. Des.* **2016**, *107*, 372–377. [[CrossRef](#)]
39. Chen, Q.; Zhu, R.; Zhu, Y.; Liu, J.; Zhu, L.; Ma, L.; Chen, M. Adsorption of polyhydroxy fullerene on polyethyleneimine-modified montmorillonite. *Appl. Clay Sci.* **2016**, *132–133*, 412–418. [[CrossRef](#)]
40. Nchoe, O.B.; Ntuli, T.D.; Klink, M.J.; Mtunzi, F.M.; Pakade, V.E. A comparative study of acid, base and Fenton-like reagent treated biomass for Cr(VI) sequestration from aqueous solutions. *Water Environ. Res.* **2020**, *93*, 370–383. [[CrossRef](#)]
41. Yan, Y.; An, Q.; Xiao, Z.; Zheng, W.; Zhai, S. Flexible core-shell/bead-like alginate@PEI with exceptional adsorption capacity, recycling performance toward batch and column sorption of Cr(VI). *Chem. Eng. J.* **2017**, *313*, 475–486. [[CrossRef](#)]
42. Zhao, D.; Gao, X.; Wu, C.; Xie, R.; Feng, S.; Chen, C. Facile preparation of amino functionalized graphene oxide decorated with Fe₃O₄ nanoparticles for the adsorption of Cr(VI). *Appl. Surf. Sci.* **2016**, *384*, 1–9. [[CrossRef](#)]
43. Chen, Y.; Wang, B.; Xin, J.; Sun, P.; Wu, D. Adsorption behavior and mechanism of Cr(VI) by modified biochar derived from *Enteromorpha prolifera*. *Ecotoxicol. Environ. Saf.* **2018**, *164*, 440–447. [[CrossRef](#)]

44. Chang, J.; Wang, H.; Zhang, J.; Xue, Q.; Chen, H. New insight into adsorption and reduction of hexavalent chromium by magnetite: Multi-step reaction mechanism and kinetic model developing. *Colloids Surfaces A Physicochem. Eng. Asp.* **2021**, *611*, 125784. [[CrossRef](#)]
45. Nkutha, C.S.; Diagboya, P.N.; Mtunzi, F.M.; Dikio, E.D. Application of eco-friendly multifunctional porous graphene oxide for adsorptive sequestration of chromium in aqueous solution. *Water Environ. Res.* **2020**, *92*, 1070–1079. [[CrossRef](#)]
46. Pakade, V.E.; Maremeni, L.C.; Ntuli, T.D.; Tavengwa, N.T. Application of quaternized activated carbon derived from macadamia nutshells for the removal of hexavalent chromium from aqueous solutions. *S. Afr. J. Chem.* **2016**, *69*, 180–188. [[CrossRef](#)]
47. Niazi, L.; Lashanizadegan, A.; Sharififard, H. Chestnut oak shells activated carbon: Preparation, characterization and application for Cr (VI) removal from dilute aqueous solutions. *J. Clean. Prod.* **2018**, *185*, 554–561. [[CrossRef](#)]
48. Qhubu, M.C.; Mgidlana, L.G.; Madikizela, L.M.; Pakade, V.E. Preparation, characterization and application of activated clay biochar composite for removal of Cr(VI) in water: Isotherms, kinetics and thermodynamics. *Mater. Chem. Phys.* **2021**, *260*, 124165. [[CrossRef](#)]
49. Yang, Y.; Chen, N.; Feng, C.; Li, M.; Gao, Y. Chromium removal using a magnetic corncob biochar/polypyrrole composite by adsorption combined with reduction: Reaction pathway and contribution degree. *Colloids Surfaces A Physicochem. Eng. Asp.* **2018**, *556*, 201–209. [[CrossRef](#)]
50. Zhang, X.; Lv, L.; Qin, Y.; Xu, M.; Jia, X.; Chen, Z. Removal of aqueous Cr(VI) by a magnetic biochar derived from Melia azedarach wood. *Bioresour. Technol.* **2018**, *256*, 1–10. [[CrossRef](#)]
51. Larraza, I.; López-González, M.; Corrales, T.; Marcelo, G. Hybrid materials: Magnetite-Polyethylenimine-Montmorillonite, as magnetic adsorbents for Cr(VI) water treatment. *J. Colloid Interface Sci.* **2012**, *385*, 24–33. [[CrossRef](#)] [[PubMed](#)]
52. Lima, E.C.; Hosseini-Bandegharai, A.; Moreno-Piraján, J.C.; Anastopoulos, I. A critical review of the estimation of the thermodynamic parameters on adsorption equilibria. Wrong use of equilibrium constant in the Van't Hoof equation for calculation of thermodynamic parameters of adsorption. *J. Mol. Liq.* **2019**, *273*, 425–434. [[CrossRef](#)]
53. Zhang, Y.; Xu, M.; Li, H.; Ge, H.; Bian, Z. The enhanced photoreduction of Cr(VI) to Cr(III) using carbon dots coupled TiO₂ mesocrystals. *Appl. Catal. B Environ.* **2018**, *226*, 213–219. [[CrossRef](#)]
54. Tran, H.N.; You, S.J.; Chao, H.P. Thermodynamic parameters of cadmium adsorption onto orange peel calculated from various methods: A comparison study. *J. Environ. Chem. Eng.* **2016**, *4*, 2671–2682. [[CrossRef](#)]
55. Hokkanen, S.; Bhatnagar, A.; Repo, E.; Lou, S.; Sillanpää, M. Calcium hydroxyapatite microfibrillated cellulose composite as a potential adsorbent for the removal of Cr(VI) from aqueous solution. *Chem. Eng. J.* **2016**, *283*, 445–452. [[CrossRef](#)]